A combined computational and experimental study on selective flucloxacillin hydroxylation by cytochrome P450 BM3 variants

Luirink, Rosa A.; Dekker, Stefan J.; Capoferri, Luigi; Kuiper, Cynthia L.; Janssen, Laura F.H.; Ari, Mehmet E.; Vermeulen, Nico P.E.; Vos, J. Chris; Commandeur, Jan N.M.; Geerke, Daan P.

published in
Journal of Inorganic Biochemistry
2018

DOI (link to publisher)
10.1016/j.jinorgbio.2018.04.013

document version
Publisher's PDF, also known as Version of record

Journal of Inorganic Biochemistry 184 (2018) 115–122

Contents lists available at ScienceDirect

Journal of Inorganic Biochemistry

journal homepage: www.elsevier.com/locate/jinorgbio

A combined computational and experimental study on selective flucloxacillin hydroxylation by cytochrome P450 BM3 variants

Rosa A. Luirink[1], Stefan J. Dekker[1], Luigi Capoferri, Laura F.H. Janssen, Cynthia L. Kuiper, Mehmet E. Ari, Nico P.E. Vermeulen, J. Chris Vos, Jan N.M. Commandeur, Daan P. Geerke[*]

Division of Molecular and Computational Toxicology, Amsterdam Institute for Molecules, Medicines and Systems (AIMMS), Faculty of Science, Vrije Universiteit, De Boelelaan 1108, 1081 HZ Amsterdam, the Netherlands

ARTICLE INFO

Keywords:
Biocatalysis
Cytochrome P450 BM3
Docking
Flucloxacillin
Molecular Dynamics simulations

ABSTRACT

The 5′-hydroxymethyl metabolite of the penicillin based antibiotic flucloxacillin (FLX) is considered to be involved in bile duct damage occurring in a small number of patients. Because 5′-hydroxymethyl FLX is difficult to obtain by organic synthesis, biosynthesis using highly active and regioselective biocatalysts would be an alternative approach. By screening an in-house library of Cytochrome P450 (CYP) BM3 mutants, mutant *M11 L437E* was identified as a regioselective enzyme with relatively high activity in production of 5′-hydroxymethyl FLX as was confirmed by mass spectrometry and NMR. In contrast, incubation of M11 L437E and other mutants with oxacillin (OX, which differs from FLX by a lack of aromatic halogens) resulted in formation of two metabolites. In addition to 5′-hydroxymethyl OX we identified a product resulting from aromatic hydroxylation. *In silico* studies of both FLX and OX with three CYP BM3 mutants revealed substrate binding poses allowing for 5′-methyl hydroxylation, as well as binding poses with the aromatic moiety in the vicinity of the heme iron for which the corresponding product of aromatic hydroxylation was not observed for FLX. Supported by the (differences in) experimentally determined ratios of product formation for OX hydroxylation by M11 and its L437A variant and M11 L437E, Molecular Dynamics simulations suggest that the preference of mutant M11 L437E to bind FLX in its catalytically active pose over the other binding orientation contributes to its biocatalytic activity, highlighting the benefit of studying effects of active-site mutations on possible alternative enzyme-substrate binding poses in protein engineering.

1. Introduction

Flucloxacillin (FLX) is a synthetic antibiotic with the penicillin core structure (Fig. 1A) and belongs to the class of penicillinase-resistant isoxazolyl penicillins [1,2]. FLX is used in the treatment of Staphylococcal infection. Its use is associated with rare cases of idiosyncratic drug induced liver injury (IDILI, predominantly cholestatic), with a higher incidence in women and elderly [3,4]. Because of its widespread use FLX has been reported to be one of the most common causes of severe and even fatal IDILI [5].

Although the mechanism of FLX-induced IDILI is not yet fully understood, it is accepted that certain polymorphisms of the immune system, in particular HLA-B*5701, strongly increase the risk for IDILI [6,7]. Although the association with HLA-B*5701 is one of the strongest ever reported, only 0.1% of the patients with this genotype will eventually develop FLX-induced IDILI [6]. It is therefore likely that other factors are involved in the susceptibility to cholestasis as well. Because the metabolite of FLX appeared much more toxic to biliary epithelial cells than FLX itself, variability in metabolism of FLX may also determine susceptibility to FLX-induced DILI [8].

FLX is mainly metabolized by Cytochrome P450 (CYP) 3A4 to 5′-hydroxymethyl FLX (Fig. 1B) [2]. To our knowledge, no synthetic route for 5′-hydroxymethyl FLX has been published yet and only the use of liver microsomes from rats treated with dexamethasone has been reported as a method to obtain 5′-hydroxymethyl FLX at analytical scale [8]. However, liver microsomes have intrinsically low activity of CYPs and require animals as source of microsomes and are therefore less suitable for biosynthetic approaches. As an alternative to liver microsomes, CYP BM3 (CYP102A1) from *Bacillus megaterium* has more perspective for biosynthesis, since it is the CYP with one of the highest reported turnovers [9,10]. Whereas wild-type (WT) BM3 only accepts long fatty acids as substrates, many successful protein engineering

* Corresponding author.
E-mail address: d.p.geerke@vu.nl (D.P. Geerke).
[1] Contributed equally.

https://doi.org/10.1016/j.jinorgbio.2018.04.013
Received 16 December 2017; Received in revised form 23 March 2018; Accepted 18 April 2018
Available online 24 April 2018
0162-0134/

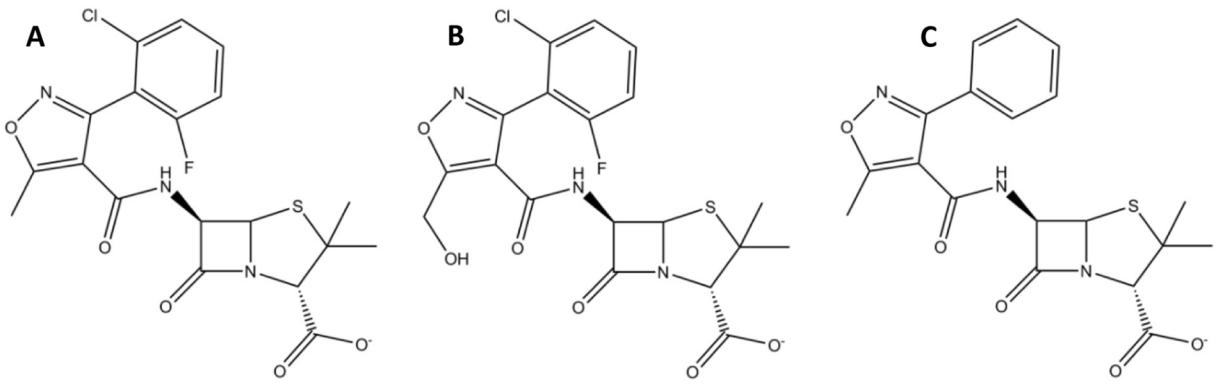

Fig. 1. (A) Flucloxacillin (FLX). **(B)** 5′-hydroxymethyl FLX. **(C)** Oxacillin (OX).

studies have been reported over the last years that report mutants of BM3 able to hydroxylate drugs and drug-like compounds with high activity and with regio- and/or stereo-selectivity [11–21]. However, rationally predicting novel mutants with enhanced selectivity and/or activity is still difficult especially when considering the flexibility of their active site and because they can typically bind a variety of substrates in multiple binding poses [18,22–26]. In the present combined experimental and computational study we report and study the biocatalytic activity for (regioselective) 5′ methyl-hydroxylation of FLX by CYP BM3 mutants *M11*, *M11 L437E* and *M11 L437A*. M11 is a mutant capable of metabolizing a variety of drug-like or other industrially relevant substrates [25,27–29] and contains mutations R47L/E64G/F81I/F87V/E143G/L188Q/Y198C/E267V/H285Y/G415S with respect to wild-type BM3 [30]. Our *in silico* studies suggest that the L437E mutation favors binding of FLX in its catalytically active binding pose over substrate binding in a less reactive binding mode. This illustrates the relevance to consider alternative enzyme-substrate binding poses as well when designing promiscuous biocatalysts such as BM3 variants. We could support these findings by incubations of M11 and its 437E and 437A mutants with oxacillin (OX), which only differs from FLX by the aromatic Cl and F substituents of the latter (Fig. 1).

2. Methods

2.1. Chemicals

FLX was kindly supplied by dr. Bayliss (University of Liverpool) and OX was acquired from Sigma Aldrich (Zwijndrecht, the Netherlands; purity: 99%). All other chemicals were obtained from standard suppliers and of analytical grade.

2.2. Mutagenesis and expression of BM3 mutants

Mutant M11 L437A was cloned using the primers listed in Table 1 according to the quick change protocol as published previously [28]. Constructs for wild-type BM3 [31] and the BM3 mutants M01, M02, M05, M11, M01 L437E, M11 L437E, M11 L437N, M11 L437S, M11 L437T [21], M01 S72D, M01 S72E, M01 A74D, M01 A74E [28], M01 S72I, M01 A82W, M11 S72D, M11 A82W V87F, M11 A82W L437N, M11 V87F L437 N, M11 V87F L437S, M11 V87I L437N, M11 V87I L437S [32], M11 V87A, M11 V87G, M11 V87H and M11 V87I [33] have been reported before. Enzyme expression was conducted as described in reference [28], except that after expression cells were lysed with three rounds in an Avastin EmulsiFlex-C3 instead of a French Press. In a next step, M11, M11 L437E and M11 L437A were purified over Ni-NTA beads according to a protocol reported before [21]. Enzyme concentrations were determined by CO-specs according to the protocol of Omura and Sato [32].

2.3. Incubations

For biotransformation reactions, lysates containing 200 nM of BM3 mutants or 2 mg/mL dexamethasone induced rat liver microsomes were incubated with 250 μM FLX or OX in 100 mM potassium phosphate buffer pH 7.4 (KPi pH 7.4) in the presence of an NADPH-regenerating system (NRS).

The NRS consisted of 100 μM $NADP^+$, 10 mM glucose-6-phosphate, and 0.5 units/mL glucose-6-phosphate dehydrogenase. Reactions were started by the addition of NRS and were performed at 24 °C for BM3 or 37 °C for rat liver microsomes. To compare the different BM3 mutants in the initial screen, the incubations were performed for 1 h. For a selection of BM3 mutants, enzyme kinetic parameters were determined by incubating with different concentrations of FLX and OX. For enzyme kinetic analysis, an incubation time of 10 min was used during which metabolite formation was found to be linear in time [data not shown]. The reaction was stopped by addition of an equal volume of ice-cold methanol containing 2% acetic acid to prevent hydrolysis of the β-lactam ring. Proteins were removed by centrifugation at 20,800*g* for 20 min. The supernatant was analyzed by HPLC-UV and the identity of the metabolites was confirmed by LC-MS. Michaelis-Menten parameters were obtained by nonlinear regression using GraphPad Prism 5.00 (Graphpad Software, San Diego, CA, USA). Kinetics for M11 L437E and M11 L437A were fitted to the Michaelis-Menten function, while M11 kinetics were fitted to the substrate inhibition function (with obtained K_i = 4.0 mM) as described by Copeland in Eq. (5.44) of reference [33], which assumes an inactive ternary substrate-enzyme-substrate (SES) complex.

2.4. Preparative scale incubations

For preparative scale metabolite production, 100 mL 100 mM KPi pH 7.4 containing 1 μM BM3, 2 mM substrate and NRS was incubated at

Table 1
Forward (fw) and reverse (rv) primers used to mutate position L437. The introduced silent restriction site BsmA1 is underlined and the mutated residues are highlighted in bold.

	Sequence
L437A fw primer	5′-CTACGAGCTCGATATTAAAGAGACT**GCT**ACGTTAAAACCTGAAGGCTTTGTGG-3′
L437A rv primer	5′-CCACAAAGCCTTCAGGTTTTAACGT**AGC**AGT**C**TCTTTAATATCGAGCTCGTAG-3′

room temperature with constant agitation by a steering bean. For the production of 5′-hydroxymethyl FLX, M11 L437E was used, whereas for the hydroxylation of OX M11 was used. Fresh BM3 mutant and NRS were added every hour for 7 h and once more after 20 h. The reaction was terminated after 24 h by the addition of an equal volume ice-cold methanol containing 2% acetic acid and centrifuged at 4600*g* for 2 h at 4 °C. Next, the methanol was evaporated and the sample concentrated by vacuum centrifuging and the metabolites were purified from the supernatant by preparative HPLC. 5′-hydroxymethyl-OX was identified by ^{1}H NMR and 5′-hydroxymethyl-FLX was identified by ^{1}H and ^{19}F NMR. The aromatic hydroxylation of OX was identified by LC-MS/MS.

2.5. Analytical methods

Metabolite formation for FLX and OX was assessed on a Shimadzu HPLC equipped with two LC-20AD pumps, an SPD20A UV-detector set to 272 nm, and a SIL20AC auto-sampler. Separation was performed on a Luna 5 µm 4.6 × 150 mm C-18 column with a binary gradient consisting of eluents A (0.1 v/v% formic acid, 1 v/v% acetonitrile and 98.9 v/v% H_2O) and B (0.1 v/v% formic acid, 98.9 v/v% acetonitrile and 1 v/v% H_2O) at 0.5 mL/min. The gradient went from 40 v/v% to 99 v/v% B in 23.5 min, after which the percentage went back to 40% B in 0.5 min. The column was equilibrated for 11 min before a next sample was injected.

An Agilent 1200 rapid resolution LC system connected to an Agilent TOF 6230 mass spectrometer with an electrospray ionization source was used to determine the mass of the metabolites. 3500 V 10 L/min nitrogen drying gas together with 50 psig nitrogen nebulizing gas at 350 °C were used and the capillary was set to 3500 V. For MS/MS an Agilent QTOF 6500 was used with a collision energy of 10 V. The LC column and gradient were identical to the HPLC-UV set-up.

2.6. Preparative HPLC

The preparative HPLC system was similar to the one described above, but with a Shimadzu LC-20AB pump and a FRC-10A fraction collector connected. Samples consisting of 1 mL sample were injected into an Xbridge prep C18-MS (5 µm 10 × 50 mm). The same eluents as described above were used in a binary gradient going from 25% to 50% eluent B in 11 min for FLX, and from 20% to 50% eluent B for OX. Then it went back to the starting conditions and equilibrated again for 4.5 min. The flow rate was 3 mL/min. Afterwards the collected fractions were evaporated to dryness and stored at −20 °C.

2.7. ^{19}F and ^{1}H NMR spectroscopy

NMR spectra for FLX, OX and their metabolites were measured in deuterated DMSO-d_6 (Sigma Aldrich, Zwijndrecht, Netherlands) on a Bruker Avance 500 (Fallanden, Switzerland) at room temperature, equipped with a cryoprobe operating at 500.13 MHz. For identification of FLX metabolites, ^{19}F spectra and ^{1}H of FLX were compared to Keun et al. [34]

2.8. Dissociation constant measurements

To determine dissociation constants of the binding of FLX and 5′-hydroxymethyl FLX to BM3 mutants, binding spectra of the substrate-protein and metabolite-protein complexes were acquired as published previously [21]. The compounds were titrated into a cuvette containing 1 mL of 100 mM KPi pH 7.4 and 1 µM BM3 up to a final additional volume of not more than 2% of the initial solution volume. UV/Vis difference spectra were obtained on a Shimadzu UV-250IP spectrophotometer (Shimadzu Duisburg, Germany) at 24 °C. The substrate-free sample was subtracted from all following acquired spectra. The difference in absorption between 422 nm and 390 nm was plotted and analyzed by nonlinear regression fitting the data to the *one site – specific binding with hill slope* function of GraphPad Prism 5.00 (Graphpad Software, San Diego, CA, USA) to obtain the reported K_D values.

2.9. Molecular docking

The heme domain of mutant BM3 M11 was modelled using chain B of the M11 crystal structure (PDB ID 5E9Z) [26]. Missing residue Q73 and missing atoms of residues K31, Q73, K94, K97, Q109, Q110, D136, K187, K218, Q229, T245, R255, Q288, K306, K449 were added with Modeller 9.3 [35]. The structure was then steepest-descent energy minimized and protonated using the Reduce tool from the AmberTools package [36]. The protonated M11 structure was used as a docking template for FLX and OX.

FLX was first energy minimized according to the MMFF94 force field [37] with Open Babel 2.3.9 [38]. Partial atomic charges for FLX for use in MD were obtained with GAMESS (version 1 May 2012) [39] at the Hartree-Fock level using the 6-31G* basis set. Subsequently, the structure was energy minimized at the B3LYP/COSMO/6-31G* level of theory. An initial molecular structure of OX was obtained from the energy minimized FLX structure by replacing the fluorine and chlorine by hydrogens. OX was subsequently energy minimized according to the MMFF94 force field [37] with Open Babel 2.3.9 [38] as well.

The protein template and energy minimized FLX or OX structures were used in flexible docking using Protein-Ligand Ant System (PLANTS) [40] version 1.2 and the PLANTS ChemPLP scoring function [41]. To determine flexible residues, an alignment was made of the four chains of the 5E9Z crystal structure (Chains A, B, C and D) using Maestro 9.3.5 (Schrödinger Suite 2012.2) [42]. The side chains of six residues (Q73, L181, Q188, Q403, L437 and T438) were treated flexible during docking. The center of docking was placed in the middle of the active site with a distance of 0.68 nm from the heme iron along the vector connecting the heme iron with the coordinating sulfur atom of C458. The docking radius was set as 1.5 nm from the center of the docking sphere. The 300 highest-ranked docked structures were retained. Based on visual inspection, two types of binding poses were identified, designated as poses 1 and 2, respectively (see Results and discussion section). From both types of binding modes, 4–6 FLX binding poses (with the substrate's amide bond in *trans* conformation) were selected based on visual inspection and used as starting structures for separate MD simulations (50 ns production, see below for settings). For every combination of mutant and type of pose, the simulation with lowest root-mean-square deviation (RMSD) of the ligand heavy-atom positions with respect to the MD starting structure was identified as the most stable one, and this simulation was used for further analyses.

2.10. Molecular Dynamics (MD) simulations

Mutations on position 437 were introduced into the crystal structure of the M11 heme domain [26] with Modeller version 9.3 [35], after which two residues on each site of the mutated residue were allowed to reorganize in order to reduce possible steric clashes. Partial charges for the substrate atoms were obtained as described above and other interaction parameters for FLX were used from the General Amber Force Field [43], obtained by using Antechamber version 1.27 [44]. Gromacs version 5.1.1 was used for all simulations [45]. The Amber99SB-ILDN force field [46] was used to describe the protein. Unless noted otherwise, results are presented and discussed for simulations with the heme moiety in its penta-coordinated resting state. In addition, simulations with the heme modelled as Compound I (Cpd I) were performed in which the ferryl oxygen atom was placed along the normal to the heme plane at a distance of 0.164 nm from the iron atom. To describe both the heme resting-state and Cpd I, force field parameters were employed from reference [47].

Every complex was solvated in a dodecahedral box with approximately 14,500 TIP3P water molecules [48] and 14 sodium ions (15 sodium ions for M11 437E simulations) were added to neutralize the

charge of the systems. The systems were energy minimized (steepest-descent) and heated up to 300 K in three 250 ps *NVT* simulations at 100, 200 and 300 K, in which protein-backbone C_α atoms were positionally restrained with harmonic potentials with force constants of 10,000, 5000, and 50 kJ nm^{-2} mol^{-1}, respectively. Afterwards, 50.25 ns of (unrestrained) *NpT* simulations were carried out at 1 atm and 300 K. The first 0.25 ns of these production runs were discarded for further analyses. A time step of 2 fs was used, and bond lengths involving hydrogen atoms were constrained using the LINCS algorithm, with the highest order in the expansion of the constraint coupling matrix set to 4 [49]. A Langevin integrator was used with the friction coefficient for each particle calculated as mass/0.1 ps. A Berendsen barostat [50] was used to maintain the pressure close to its reference value during *NpT* simulations, with a coupling time of 0.5 ps and an isothermal compressibility of 4.5×10^{-5} bar^{-1}. Van der Waals and short-range electrostatic interactions were explicitly evaluated every time step for pairs of atoms within 0.9 nm of each other, using a grid-based pairlist that was updated every five time steps. Long-range electrostatic interactions were calculated every time step, according to the smooth particle mesh Ewald method [51] with a grid spacing of 0.125 nm. Linear center of mass motion removal took place every 5 time steps. All simulations were performed twice, in independent runs that started with different randomly assigned atomic velocities. Atomic positions and energies were stored every 2 ps for further analyses. Snapshot images were made with VMD (version 1.9.2) [52]. RMSDs in atomic positions were determined with respect to MD starting poses, and interatomic distance and RMSD time series were plotted with matplotlib, with running averages over 200 ps. Interaction profiles between ligands and the mutants were analyzed in terms of protein-ligand interaction frequencies using an in-house Python script to identify interaction types, using rule-based protocols described in the supplementary information of reference [53].

3. Results and discussion

3.1. Identification of catalytically active BM3 mutants

To identify BM3 mutants that can serve as a biocatalyst for the synthesis of 5′-hydroxymethyl FLX, first the activity screening of an in-house library of BM3 mutants was performed (see Fig. S1 of the Supplementary Information) [27,54]. For all active mutants tested only one metabolite was found with *m/z* of 470.1 $[M + H]^+$ corresponding with hydroxylation of FLX (Fig. S2A). Using ^{19}F and ^{1}H spectra NMR this metabolite was identified as 5′-hydroxymethyl FLX. The spectra obtained (Fig. S3 and S4) were consistent to the ^{19}F and ^{1}H spectra reported previously by Keun et al. [34] From our library screening (Fig. S1), mutant M11 L437E was identified as the most active mutant for FLX conversion. Enzyme kinetic analysis showed similar V_{max} values for M11 L437E and its parent M11 mutant (Fig. 2, Table 2) but M11

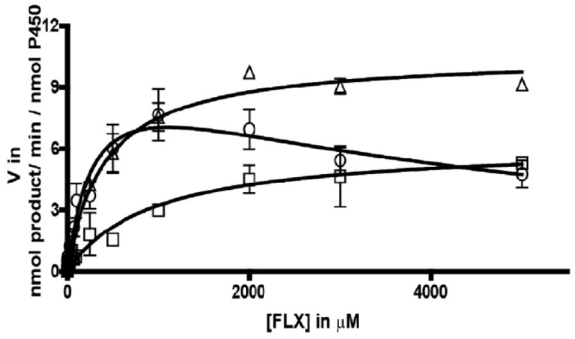

Fig. 2. Michaelis-Menten kinetics for M11 (circles), M11 L437E (triangles) and M11 L437A (squares). Data depict the mean of one experiment performed in duplo (± SD).

Table 2
Michaelis-Menten parameters V_{max} and K_m as obtained for the metabolism of FLX to 5′-hydroxymethyl flucloxacillin by BM3 mutants M11, M11 L437E and M11 L437A, and substrate inhibition constant K_i for M11.

	V_{max} (nmol product/min/nmol CYP)	K_m (μM)	K_i (mM)
M11	11.0 ± 1.9	307 ± 104	4.0 ± 0.2
M11 L437E	10.5 ± 0.5	404 ± 82	–
M11 L437A	6.2 ± 0.6	922 ± 270	–

Table 3
UV/Vis determined dissociation constants K_D and H-coefficients for the binding of FLX to BM3 mutants M11, M11 L437E and M11 L437A.

	K_D (μM)	*H-coefficient*
M11	18.6 ± 4.0	1.1 ± 0.3
M11 L437E	36.9 ± 1.6	1.7 ± 0.1
M11 L437A	34.7 ± 4.8	1.0 ± 0.1

displayed a decrease in activity at higher substrate concentrations indicating substrate inhibition and formation of an inactive SES complex [33]. UV/Vis binding studies of M11 L437E showed a higher K_D value when compared to M11 (Table 3, Fig. S5) and an H-coefficient higher than 1 indicating positive cooperativity, which was not observed for M11. For another M11 437 mutant, M11 L437A, we found a similar K_D value but a lower V_{max} value when compared to M11 L437E, Fig. 2 and Tables 2 and 3. The values for and trends in the kinetically determined K_m of the BM3 mutants differ significantly from those observed for K_D in our binding measurements, Tables 2 and 3. Assuming that binding and unbinding constants k_1 and k_{-1} are the same, this suggests that the catalytic constant k_2 may be much larger than k_{-1}. It should be realized however that K_m is determined based on the concentration-dependence of the enzyme reaction in which the iron atom is in a Fe^{2+}-state and interacts with an oxygen atom, while K_D is determined based on the concentration-dependence of the spin-state of the enzyme in which the iron is in a Fe^{3+}-state. Differences between K_m and K_D (of up to 50–100 fold) have been reported previously for other CYP enzymes as well [55].

Interestingly, after incubating OX with the M11, M11 L437E and M11 L437A mutants, two different metabolites were observed, both with the predicted *m/z* of 418.1 $[M + H]^+$ (Fig. S2B). ^{1}H NMR analysis showed that one of the metabolites was the 5′-hydroxymethyl metabolite, *cf.* Fig. S6. The second metabolite was identified by MS/MS as a product of aromatic hydroxylation: the characteristic fragment of *m/z* 243 caused by fragmentation of the β-lactam ring [56] increased in mass by *m/z* 16 upon hydroxylation, while the second fragment with an m/z of 160 did not (Fig. S7). This indicates that the incorporated oxygen atom is located at the aromatic ring of OX. Fig. 3 shows that introducing the glutamate mutation at the distant active-site position 437 leads to a reduction of total OX conversion. At low substrate concentrations we did not observe a decrease in product formation for FLX upon introducing the L437E mutation, Fig. 2. In the remainder we performed protein-structure based modeling and MD simulations to obtain more insight into the effects of the 437E mutation on substrate binding and conversion.

3.2. Substrate docking

Docking revealed two major binding poses of FLX with a C—H bond carbon atom within 0.6 nm of the heme iron, which was previously used as cut-off to identify possible catalytically-active binding orientations [57]. When docking FLX into the M11 binding pocket, 11% of the docked poses was found with the 5′ methyl carbon atom within 0.6 nm of the heme iron, whereas in 30% of the poses the phenyl ring of FLX was found to be in closest proximity of the heme iron. These two

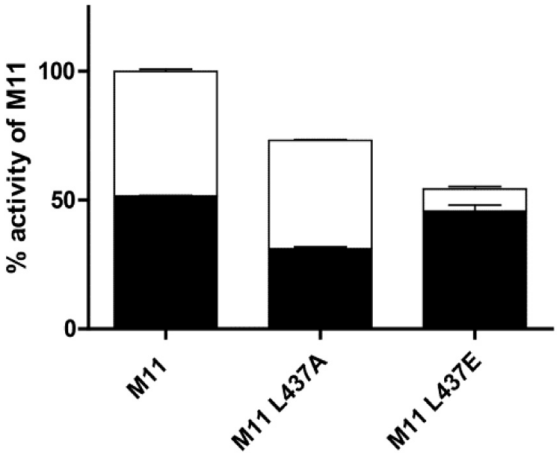

Fig. 3. Oxacillin metabolite formation by BM3 mutants M11, M11 L437A and M11 L437E. White bars depict aromatic hydroxylation of oxacillin and black bars depict 5′-hydroxymethyl oxacillin formation. Total metabolite formation of M11 is set to 100% and the data show the mean (± SD) for one experiment performed in duplo.

types of binding poses are in the remainder designated as binding pose 1 and 2, respectively, and used as starting points of our MD simulations of FLX in M11, M11 L437A and M11 L437E. Similar results were obtained when docking OX in M11. In 13% of the docked poses the 5′ methyl carbon atom of OX was within 0.6 nm of the heme iron, and in 30% of the OX binding modes the phenyl ring was closest to the heme iron.

Binding of FLX in pose 1 can lead to 5′-methyl hydroxylation, since this methyl group is in close contact with the heme iron (*cf.* Fig. 4A and B). In pose 2, the aromatic *para*-carbon atom is typically in closest vicinity of the heme iron, Fig. 4C. The FLX halogens at *meta*-position from this carbon can have a detrimental effect on intrinsic reactivity, in line with results from QM studies by Bathelt et al. on the effects of (single) halogen substituents on C—H bond activation showing an increase of several kJ/mol per *meta* halogen substitution [58]. This can explain our finding that in contrast to OX, no aromatic hydroxylation was observed for FLX, also when considering that docking results for pose 2 only show small differences in the distributions of C—Fe distances between OX and FLX (Fig. S8), suggesting that steric hindrance due to the halogen groups is not on the basis of a lack of aromatic hydroxylation of FLX upon binding in pose 2.

3.3. Molecular Dynamics simulations

MD simulations starting from pose 1 showed only small fluctuations in the relatively low RMSD of the heavy-atom positions of the substrate in the M11 and M11 L347E simulations and in one of the M11 L437A simulations (Fig. 5A). Together with our finding that the distance between the 5′ methyl carbon site-of-metabolism and Fe is constantly well below 0.6 nm in simulation (Fig. 6A), this indicates that pose 1 is stable in the mutants. Binding pose 1 was also found to be stable in the simulations with the heme group modelled as Cpd I, with average distances between a (*i.e.*, the closest) 5′ methyl hydrogen and the ferryl oxygen of less than 0.3 nm and average angles of approach of this methyl hydrogen to Fe═O on the order of 120 degrees, respectively (Supplemental Table S1). These values are close to typical values reported for transition states for CYP mediated aliphatic hydroxylation [59,60]. Table S1 also shows that no significant differences were found among the different mutants, suggesting that differences in binding orientation and C—H bond activation energy are not on the basis of the observed trends in FLX conversion rates described in Section 3.1.

As can be seen from protein residue-ligand interaction profiles obtained from MD (Figs. S9–S12), FLX is engaged in more and/or more frequent polar interactions with M11 L437E when compared to M11 or M11 L437A. In the L437E mutant, the COO^- moiety of FLX shows anionic hydrogen bonding to both the S72 and S332 residues during MD (Figs. 4B, 7A, 7B, S10), whereas only one of these interactions is formed during simulations of the other mutants (Figs. 4A, 7A, 7B, S9, S11). Note that in one of the M11 L437E simulations a Ser-COO-interaction was lost after 25 ns but a third independent MD simulation additionally confirmed the possibility of FLX interacting with both serines, Fig. S12. Another interaction between FLX and M11 L437E which was not observed in the M11 and M11 L437A simulations involved K69 interacting with the beta-lactam oxygen of FLX (Figs. S9–S12)·The simultaneous interaction between the FLX COO^- group and S72 and S332 and the interaction with K69 may be induced by repulsion between the substrate's and E437's anionic groups, as suggested by the small change in binding orientation towards S332 in M11 L437E with respect to M11 (Fig. 4A and B) and by the substrate-binding induced interaction between E437 and Q188 (Figs. 7C and 4B). Whereas the anionic repulsion can negatively affect total FLX binding to M11 L437E when compared

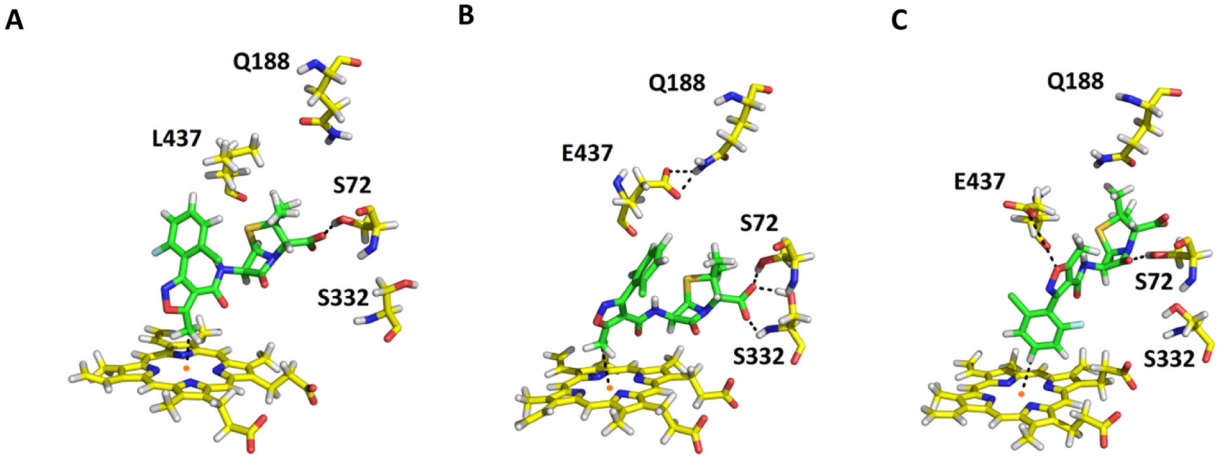

Fig. 4. Binding orientations of FLX (in green) observed during MD. Heme group (yellow) and residues S72, Q188, L/E437 and S332 (yellow) are explicitly shown in stick representation as well. Selected interactions/contacts are represented with dashed lines. **(A)** Representative FLX binding pose 1 in M11. Interactions/contacts depicted are between FLX′ 5′ methyl carbon and the heme iron, and between a FLX′ carboxyl oxygen and the S72 side-chain hydroxyl group. **(B)** Representative FLX binding pose 1 in M11 L437E, interactions/contacts depicted are between FLX′ carboxyl oxygens and S332's backbone nitrogen or S332's and S72's side-chain hydroxyl groups, and between the E437 carboxyl oxygens and Q188 nitrogen. **(C)** FLX binding pose 2 in M11 L437E, interactions/contacts depicted are between FLX′ phenyl *para*-carbon and heme iron, between E437's carboxyl and FLX' ring oxygen, and between FLX′ lactam oxygen and S72's side-chain hydroxyl group.

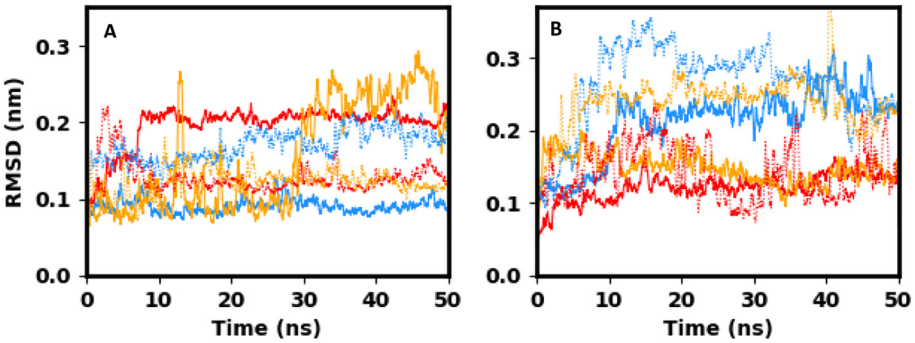

Fig. 5. Time series of heavy-atom positional root-mean-square deviations (RMSDs) of FLX in BM3 mutants M11 (red), M11 L437E (blue) and M11 L437A (yellow), as obtained from MD simulations starting from binding pose 1 **(A)** or binding pose 2 **(B)**. Results from independent MD simulations per system are shown by solid and dotted lines, respectively.

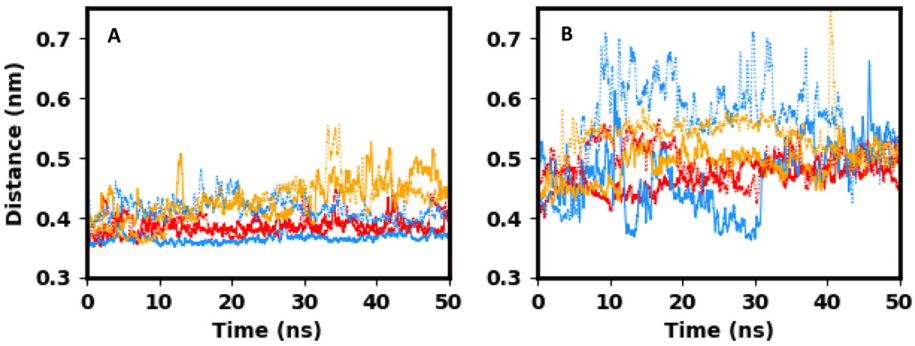

Fig. 6. Time series during MD simulations of FLX in M11 (red), M11 L437E (blue) and M11 L437A (yellow) for the distance between FLX 5′-methyl carbon atom and the heme iron as obtained from MD simulations starting from binding pose 1 **(A)**, and for the distance between the heme iron and the FLX carbon atom at para position (meta position with respect to the aromatic halogen substituents) as obtained from MD simulations starting from binding pose 2 **(B)**. Results from independent MD simulations per system are shown by solid and dotted lines, respectively.

to M11 or M11 L437A, the observed interaction with S72, S332 and K69 will have a stabilizing effect on substrate binding in pose 1 in the L437E mutant.

The stabilizing hydrogen bonds of FLX with S332 and K69 in the L437E mutant are not observed when simulating FLX in binding pose 2 (Fig. 4C and S14). A hydrogen bond between the S72 side-chain OH group and the lactam oxygen of FLX is present during simulation in M11 and in the L437A and L437E mutants, *cf.* Fig. 4C and Figs. S13–S15. Also another hydrogen bond is formed between Y51 and the FLX COO-group in all simulations involving binding pose 2 (Figs. S13–S15) except in one of the runs in M11 L437E (Fig. S14B). Simulations starting from binding pose 2 show a higher substrate RMSD and larger fluctuations of the RMSD (Fig. 5B) in M11 L437E than in M11 and one run of M11 L437A. This suggests that the L437E mutation destabilizes binding pose 2, as supported by the large fluctuation in the distance between the heme iron and aromatic *para* carbon in the M11 L437E simulations, Fig. 6B. Destabilization of pose 2 in L437E can be due to electrostatically unfavorable contacts between E437's anionic group and the partially negatively charged oxygen and nitrogen atoms in the central 5-ring of FLX (Fig. 4C), in line with higher average protein-substrate electrostatic interaction energies obtained for pose 2 binding to M11 L437E when compared to results from simulations in M11 and M11 L437A, Table 4. For M11 and M11 L437A, favoring factors for FLX binding in pose 1 over pose 2 were not observed.

Table 4
Average FLX-protein electrostatic interaction energies (in kJ/mol) as obtained from MD simulations of BM3 mutants M11, M11 L437A and M11 L437E in complex with FLX binding in pose 1 or pose 2.

	M11	M11 L437A	M11 L437E
Pose 1	−73.3	−72.0	−200.1
Pose 2	−86.7	−94.7	−71.2

Based on these findings we hypothesize that M11 L437E preferably binds FLX in pose 1 and that pose 2 may contribute more substantially to M11 and M11 L437A binding. Since no aromatic site-of-metabolism (SOM) was identified for FLX, binding in pose 2 can have a detrimental and inhibitory effect on metabolite formation for this substrate. Our suggestion that this effect is a result of low intrinsic reactivity, and not due to possible hindrance for transition state formation by the halogen substituents (Section 3.2) is supported by our Cpd I simulations with FLX bound in pose 2. In M11 L437A and in one of the simulations of M11 and M11 L437E, the *para* carbon was found to be able to adapt an

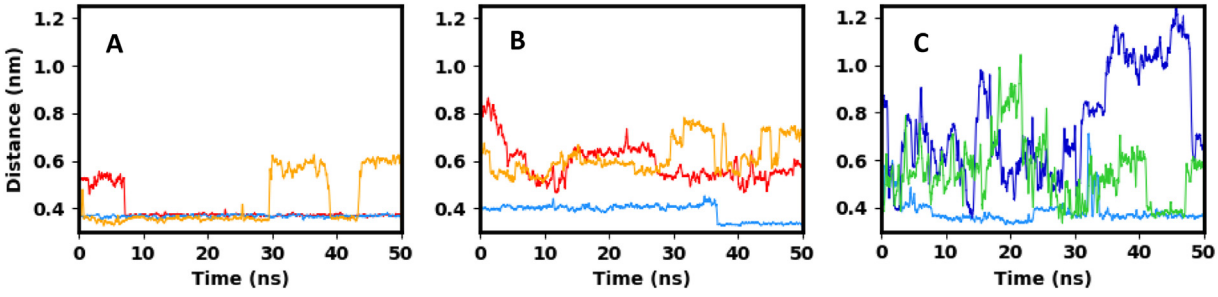

Fig. 7. Time series during MD simulations of FLX in M11 (red), M11 L437E (blue) and M11 L437A (yellow) for the minimum distance between FLX' carboxylate carbon atom and Ser72 atoms **(A)**, and for the minimum distance between FLX' carboxylate carbon atom and Ser332 atoms **(B)**; and time series during MD simulations of M11 437E in complex with FLX in pose 1 (light blue) or 2 (dark blue), or without substrate (green), for the distance between Q188's nitrogen atom and E437's carboxylate carbon atom **(C)**.

average distance to the ferryl oxygen which was between 0.3 and 0.4 nm, Table S2. This was previously used as criterion to select protein-substrate structures in combined quantum mechanical/molecular mechanical studies on transition state formation for aromatic C−H hydroxylation [59,60]. The possible inhibitory effect of a non-reactive binding pose was recently also described for another biocatalytic active CYP in X-ray crystallographic studies on CYP109E1 by Thunissen and co-workers [61]. Considering the similar binding modes obtained for OX and FLX, our hypothesis is supported by comparing ratios in product formation for OX conversion among the mutants, for which M11 and M11 L437A showed approximately 5-fold more aromatic hydroxylation than M11 L437E, Fig. 3.

4. Conclusions

We performed a combined computational and experimental study on selective 5′-methyl hydroxylation of FLX by CYP BM3 mutants M11, M11 L437E and M11 L437A. At substrate concentration on the order of its observed K_m value, we found comparable activity in FLX hydroxylation by CYP BM3 mutants M11 L437E and M11, but more product formation by M11 for the similar OX substrate. In line with the observed differences in product ratios for OX, our MD simulations suggest a preference for substrate binding by M11 L437E in an orientation consistent with 5′ methyl hydroxylation over an alternative binding mode. FLX binding in the latter orientation may well have a detrimental effect on product formation by M11 and M11 L437A, illustrating the relevance and potential for enzyme engineering in considering possible catalytically inactive poses as well in the prediction and fine tuning of substrate binding and conversion by malleable biocatalysts. Our simulation data could not explain the basis for substrate inhibition at higher substrate concentration as observed for M11 but not for M11 L437E and M11 L437A. Considering the relatively high activity of M11 L437E for 5′-hydroxylation of FLX it can serve as an alternative to biosynthesize 5′-hydroxymethyl FLX compared to the currently available approach using rat liver microsomes.

Abbreviations

FLX Flucloxacillin
OX Oxacillin
IDILI Idiosyncratic drug induced liver injury
Cpd I Compound I
CYP Cytochrome P450
DMSO Dimethylsulfoxide
SOM Site-of-metabolism
NRS NADPH-regenerating system
RMSD Root-mean-square deviation

Acknowledgments

This work was supported by the Netherlands Organization for Scientific Research (NWO, VIDI grant 723.012.105) and by the European Community under the Innovative Medicines Initiative (IMI) program through Grant Agreement number 115336.

Appendix A. Supplementary data

Supplementary data to this article can be found online at https://doi.org/10.1016/j.jinorgbio.2018.04.013.

References

[1] R. Sutherland, E.A. Croydon, G.N. Rolinson, Flucloxacillin, a new isoxazolyl penicillin, compared with oxacillin, cloxacillin, and dicloxacillin, Br. Med. J. 4 (1970) 455–460.
[2] R.E. Jenkins, X. Meng, V.L. Elliott, N.R. Kitteringham, M. Pirmohamed, B.K. Park, Characterisation of flucloxacillin and 5-hydroxymethyl flucloxacillin haptenated HSA in vitro and in vivo, PROTEOMICS-Clinical Appl. 3 (2009) 720–729.
[3] R. Olsson, B.E. Wiholm, C. Sand, L. Zettergren, R. Hultcrantz, M. Myrhed, Liver damage from flucloxacillin, cloxacillin and dicloxacillin, J. Hepatol. 15 (1992) 154–161.
[4] S. Russmann, J.A. Kaye, S.S. Jick, H. Jick, Risk of cholestatic liver disease associated with flucloxacillin and flucloxacillin prescribing habits in the UK: cohort study using data from the UK general practice research database, Br. J. Clin. Pharmacol. 60 (2005) 76–82.
[5] E. Björnsson, P. Jerlstad, A. Bergqvist, R. Olsson, Fulminant drug-induced hepatic failure leading to death or liver transplantation in Sweden, Scand. J. Gastroenterol. 40 (2005) 1095–1101.
[6] A.K. Daly, P.T. Donaldson, P. Bhatnagar, Y. Shen, I. Pe'er, A. Floratos, M.J. Daly, D.B. Goldstein, S. John, M.R. Nelson, HLA-B* 5701 genotype is a major determinant of drug-induced liver injury due to flucloxacillin, Nat. Genet. 41 (2009) 816–819.
[7] M.M. Monshi, L. Faulkner, A. Gibson, R.E. Jenkins, J. Farrell, C.J. Earnshaw, A. Alfirevic, K. Cederbrant, A.K. Daly, N. French, Human leukocyte antigen (HLA)-B* 57:01-restricted activation of drug-specific T cells provides the immunological basis for flucloxacillin-induced liver injury, Hepatology (2) (2013) 727–739.
[8] F. Lakehal, P.M. Dansette, L. Becquemont, E. Lasnier, R. Delelo, P. Balladur, R. Poupon, P.H. Beaune, C. Housset, Indirect cytotoxicity of flucloxacillin toward human biliary epithelium via metabolite formation in hepatocytes, Chem. Res. Toxicol. 14 (2001) 694–701.
[9] M.A. Noble, C.S. Miles, S.K. Chapman, D.A. Lysek, A.C. Mackay, G.A. Reid, R.P. Hanzlik, A.W. Munro, Roles of key active-site residues in flavocytochrome P450 BM3, Biochem. J. 339 (1999) 371–379.
[10] A.J. Warman, O. Roitel, R. Neeli, H.M. Girvan, H.E. Seward, S.A. Murray, K.J. McLean, M.G. Joyce, H. Toogood, R.A. Holt, D. Leys, N.S. Scrutton, A.W. Munro, Flavocytochrome P450 BM3: an update on structure and mechanism of a biotechnologically important enzyme, Biochem. Soc. Trans. 33 (2005) 747 LP–753.
[11] T.W. Ost, C.S. Miles, J. Murdoch, Y. Cheung, G.A. Reid, S.K. Chapman, A.W. Munro, Rational re-design of the substrate binding site of flavocytochrome P450 BM3, FEBS Lett. 486 (2000) 173–177.
[12] B.M.A. van Vugt-Lussenburg, E. Stjernschantz, J. Lastdrager, C. Oostenbrink, N.P.E. Vermeulen, J.N.M. Commandeur, Identification of critical residues in novel drug metabolizing mutants of cytochrome P450BM3 using random mutagenesis, J. Med. Chem. 50 (2007) 455–461.
[13] C.J.C. Whitehouse, S.G. Bell, H.G. Tufton, R.J.P. Kenny, L.C.I. Ogilvie, L.L. Wong, Evolved CYP102A1 (P450(BM3)) variants oxidise a range of non-natural substrates and offer new selectivity options, Chem. Commun. (2008) 966–968.
[14] J.C. Lewis, F.H. Arnold, Catalysts on demand: selective oxidations by laboratory-evolved cytochrome P450 BM3, Chimia 63 (2009) 309–312.
[15] E. Weber, A. Seifert, M. Antonovici, C. Geinitz, J. Pleiss, V.B. Urlacher, Screening of a minimal enriched P450 BM3 mutant library for hydroxylation of cyclic and acyclic alkanes, Chem. Commun. 47 (2011) 944–946.
[16] S.T. Jung, R. Lauchli, F.H. Arnold, Cytochrome P450: taming a wild type enzyme, Curr. Opin. Biotechnol. 22 (2011) 809–817.
[17] L. Wong, P450BM3 on steroids: the Swiss army knife P450 enzyme just gets better, ChemBioChem 12 (2011) 2537–2539.
[18] J. Kirchmair, M.J. Williamson, J.D. Tyzack, L. Tan, P.J. Bond, A. Bender, R.C. Glen, Computational prediction of metabolism: sites, products, SAR, P450 enzyme dynamics, and mechanisms, J. Chem. Inf. Model. 52 (2012) 617–648.
[19] V. Rea, A.J. Kolkman, E. Vottero, E.J. Stronks, K.A.M. Ampt, M. Honing, N.P.E. Vermeulen, S.S. Wijmenga, J.N.M. Commandeur, Active site substitution A82W improves the regioselectivity of steroid hydroxylation by cytochrome P450 BM3 mutants as rationalized by spin relaxation nuclear magnetic resonance studies, Biochemistry 51 (2012) 750–760.
[20] R. Agudo, G. Roiban, M.T. Reetz, Achieving regio-and enantioselectivity of P450-catalyzed oxidative CH activation of small functionalized molecules by structure-guided directed evolution, ChemBioChem 13 (2012) 1465–1473.
[21] H. Venkataraman, S.B.A. de Beer, D.P. Geerke, N.P.E. Vermeulen, J.N.M. Commandeur, Regio- and stereoselective hydroxylation of optically active alpha-ionone enantiomers by engineered cytochrome P450 BM3 mutants, Adv. Synth. Catal. 354 (2012) 2172–2184.
[22] E. Stjernschantz, N.P.E. Vermeulen, C. Oostenbrink, Computational prediction of drug binding and rationalisation of selectivity towards cytochromes P450, Expert Opin. Drug Metab. Toxicol. 4 (2008) 513–527.
[23] E. Stjernschantz, C. Oostenbrink, Improved ligand-protein binding affinity predictions using multiple binding modes, Biophys. J. (2010) 2682–2691.
[24] S.B.A. de Beer, L.A.H. van Bergen, K. Keijzer, V. Rea, H. Venkataraman, C. Fonseca Guerra, F.M. Bickelhaupt, N.P.E. Vermeulen, J.N.M. Commandeur, D.P. Geerke, The role of protein plasticity in computational rationalization studies on regioselectivity in testosterone hydroxylation by cytochrome P450 BM3 mutants, Curr. Drug Metab. 13 (2012) 155–166.
[25] S.B.A. de Beer, H. Venkataraman, D.P. Geerke, C. Oostenbrink, N.P.E. Vermeulen, Free energy calculations give insight into the stereoselective hydroxylation of alpha-Ionones by engineered cytochrome P450 BM3 mutants, J. Chem. Inf. Model. 52 (2012) 2139–2148.
[26] L. Capoferri, R. Leth, E. ter Haar, A.K. Mohanty, P.D.J. Grootenhuis, E. Vottero, J.N.M. Commandeur, N.P.E. Vermeulen, F.S. Jørgensen, L. Olsen, D.P. Geerke, Insights into regioselective metabolism of mefenamic acid by cytochrome P450 BM3 mutants through crystallography, docking, molecular dynamics, and free energy calculations, Proteins Struct. Funct. Bioinforma. 84 (2016) 383–396.
[27] B.M.A. van Vugt-Lussenburg, E. Stjernschantz, J. Lastdrager, C. Oostenbrink, N.P.E. Vermeulen, J.N.M. Commandeur, Identification of critical residues in novel

drug metabolizing mutants of cytochrome P450 BM3 using random mutagenesis, J. Med. Chem. 50 (2007) 455–461.
[28] J. Reinen, J.S. van Leeuwen, Y. Li, L. Sun, P.D.J. Grootenhuis, C.J. Decker, J. Saunders, N.P.E. Vermeulen, J.N.M. Commandeur, Efficient screening of P450 BM3 mutants for their metabolic activity and diversity towards a wide set of drug-like molecules in chemical space, Drug Metab. Dispos. 39 (2011) 1568–1576.
[29] H. Venkataraman, M.C.A. Verkade-Vreeker, L. Capoferri, D.P. Geerke, N.P.E. Vermeulen, J.N.M. Commandeur, Application of engineered cytochrome P450 mutants as biocatalysts for the synthesis of benzylic and aromatic metabolites of fenamic acid NSAIDs, Bioorg. Med. Chem. 22 (2014) 5613–5620.
[30] M.C. Damsten, B.M.A. van Vugt-Lussenburg, T. Zeldenthuis, J.S.B. de Vlieger, J.N.M. Commandeur, N.P.E. Vermeulen, Application of drug metabolising mutants of cytochrome P450 BM3 (CYP102A1) as biocatalysts for the generation of reactive metabolites, Chem. Biol. Interact. 171 (2008) 96–107.
[31] A.B. Carmichael, L. Wong, Protein engineering of *Bacillus megaterium* CYP102, Eur. J. Biochem. 268 (2001) 3117–3125.
[32] T. Omura, R. Sato, The carbon monoxide-binding pigment of liver microsomes. II solubilization, purification, and properties, J. Biol. Chem. 239 (1964) 2379–2385.
[33] R.A. Copeland, Enzymes: A Practical Introduction to Structure, Mechanisms and Data Analysis, Second edition, Wiley-VCH, New York, 2000.
[34] H.C. Keun, T.J. Athersuch, O. Beckonert, Y. Wang, J. Saric, J.P. Shockcor, J.C. Lindon, I.D. Wilson, E. Holmes, J.K. Nicholson, Heteronuclear 19F − 1H statistical total correlation spectroscopy as a tool in drug metabolism: study of Flucloxacillin biotransformation, Anal. Chem. 80 (2008) 1073–1079.
[35] B. Webb, A. Sali, Comparative protein structure modeling using Modeller, Curr. Protoc. Bioinforma. (2014) 5.6.1–5.6.32.
[36] D.A. Case, T.A. Darden, T.E. Cheatham III, C.L. Simmerling, J. Wang, R.E. Duke, R. Luo, R.C. Walker, W. Zhang, K.M. Merz, AMBER 12; University of California: San Francisco, (2012).
[37] T.A. Halgren, Merck molecular force field. I. Basis, form, scope, parameterization, and performance of MMFF94, J. Comput. Chem. 17 (1996) 490–519.
[38] N.M. O'Boyle, M. Banck, C.A. James, C. Morley, T. Vandermeersch, G.R. Hutchison, Open babel: an open chemical toolbox, J. Cheminform. 3 (2011) 1–14.
[39] M.W. Schmidt, K.K. Baldridge, J.A. Boatz, S.T. Elbert, M.S. Gordon, J.H. Jensen, S. Koseki, N. Matsunaga, K.A. Nguyen, S. Su, General atomic and molecular electronic structure system, J. Comput. Chem. 14 (1993) 1347–1363.
[40] O. Korb, T. Stèutzle, T. Exner, An ant colony optimization approach to flexible protein-ligand docking, Swarm Intell. 1 (2007) 115–134.
[41] O. Korb, T. Stützle, T.E. Exner, Empirical scoring functions for advanced protein-ligand docking with PLANTS, J. Chem. Inf. Model. 49 (2009) 84–96.
[42] Maestro, Version 9.3, Schrödinger, LLC, New York, NY, (2011).
[43] J.M. Wang, R.M. Wolf, J.W. Caldwell, P.A. Kollman, D.A. Case, Development and testing of a general amber force field, J. Comput. Chem. 25 (2004) 1157–1174.
[44] J.M. Wang, W. Wang, P.A. Kollman, D.A. Case, Automatic atom type and bond type perception in molecular mechanical calculations, J. Mol. Graph. Model. 25 (2006) 247–260.
[45] M.J. Abraham, D. Van Der Spoel, E. Lindahl, B. Hess, the GROMACS development team, GROMACS User Man. Version. 5, (2014).
[46] K. Lindorff-Larsen, S. Piana, K. Palmo, P. Maragakis, J.L. Klepeis, R.O. Dror, D.E. Shaw, Improved side-chain torsion potentials for the Amber ff99SB protein force field, Proteins-Struct. Funct. Bioinforma. 78 (2010) 1950–1958.
[47] K. Shahrokh, A. Orendt, G.S. Yost, T.E. Cheatham, Quantum mechanically derived AMBER-compatible heme parameters for various states of the cytochrome P450 catalytic cycle, J. Comput. Chem. 33 (2012) 119–133.
[48] W.L. Jorgensen, J. Chandrasekhar, J.D. Madura, R.W. Impey, M.L. Klein, Comparison of simple potential functions for simulating liquid water, J. Chem. Phys. 79 (1983) 926–935.
[49] B. Hess, H. Bekker, H.J.C. Berendsen, J.G.E.M. Fraaije, LINCS: a linear constraint solver for molecular simulations, J. Comput. Chem. 18 (1997) 1463–1472.
[50] H.J.C. Berendsen, J.P.M. van Postma, W.F. van Gunsteren, A. DiNola, J.R. Haak, Molecular dynamics with coupling to an external bath, J. Chem. Phys. 81 (1984) 3684–3690.
[51] U. Essmann, L. Perera, M.L. Berkowitz, T. Darden, H. Lee, L.G. Pedersen, A smooth particle mesh Ewald method, J. Chem. Phys. 103 (1995) 8577–8593.
[52] W. Humphrey, A. Dalke, K. Schulten, VMD: visual molecular dynamics, J. Mol. Graph. 14 (1996) 33–38.
[53] M. van Dijk, A.M. ter Laak, J.D. Wichard, L. Capoferri, N.P.E. Vermeulen, D.P. Geerke, Comprehensive and automated linear interaction energy based binding-affinity prediction for multifarious cytochrome P450 aromatase inhibitors, J. Chem. Inf. Mod. 57 (2017) 2294–2308.
[54] B.M.A. van Vugt-Lussenburg, M.C. Damsten, D.M. Maasdijk, N.P.E. Vermeulen, J.N.M. Commandeur, Heterotropic and homotropic cooperativity by a drug-metabolising mutant of cytochrome P450 BM3, Biochem. Biophys. Res. Commun. 346 (2006) 810–818.
[55] Y. Zhao, D. Wan, J. Yang, B.D. Hammock, P.R. Ortiz de Montellano, Catalytic activities of tumor-specific human cytochrome P450 CYP2W1 toward endogenous substrates, Drug Metab. Dispos. 44 (2016) 771–780.
[56] K.H.M. Larmené-Beld, M.L.M. Vries-Koenjer, P.G.J. ter Horst, W. Hospes, Development and validation of a liquid chromatography/tandem mass spectrometry method for the quantification of flucloxacillin and cloxacillin in microdialysis samples, Biomed. Chromatogr. 28 (2014) 1096–1101.
[57] C. de Graaf, C. Oostenbrink, P.H.J. Keizers, T. van der Wijst, A. Jongejan, N.P.E. Vermeulen, Catalytic site prediction and virtual screening of cytochrome P450 2D6 substrates by consideration of water and rescoring in automated docking, J. Med. Chem. 49 (2006) 2417–2430.
[58] C.M. Bathelt, L. Ridder, A.J. Mulholland, J.N. Harvey, Mechanism and structure–-reactivity relationships for aromatic hydroxylation by cytochrome P450, Org. Biomol. Chem. 2 (2004) 2998–3005.
[59] J. Oláh, A.J. Mulholland, J.N. Harvey, Understanding the determinants of selectivity in drug metabolism through modeling of dextromethorphan oxidation by cytochrome P450, Proc. Natl. Acad. Sci. 108 (2011) 6050–6055.
[60] R. Lonsdale, K.T. Houghton, J. Żurek KT, C.M. Bathelt, N. Foloppe, M.J. de Groot, J.N. Harvey, A.J. Mulholland, Quantum mechanics/molecular mechanics modeling of regioselectivity of drug metabolism in cytochrome P450 2C9, J. Am. Chem. Soc. 135 (2013) 8001–8015.
[61] I.K. Jóźwik, F.M. Kiss, Ł. Gricman, A. Abdulmughni, E. Brill, J. Zapp, J. Pleiss, R. Bernhardt, A.W.H. Thunnissen, Structural basis of steroid binding and oxidation by the cytochrome P450 CYP109E1 from *Bacillus megaterium*, FEBS J. 283 (2016) 4128–4148.